Optimization of peptide hydroxamate inhibitors of insulin-degrading enzyme reveals marked substrate-selectivity

Samer O. Abdul-Hay[†], **Amy L. Lane**[‡], **Thomas R. Caulfield**[†], **Clemence Claussin**[†], **Juliette Bertrand**[†], **Amandine Masson**[†], **Shakeel Choudhry**[†], **Abdul H. Fauq**[†], **Guhlam M. Maharvi**[†], **Malcolm A. Leissring**[†,*]

[†]Department of Neuroscience, Mayo Clinic, Jacksonville, FL 32224, United States

[‡]Department of Chemistry, University of North Florida, Jacksonville, FL 32224, United States

Abstract

Insulin-degrading enzyme (IDE) is an atypical zinc-metallopeptidase that degrades insulin and the amyloid ß-protein and is strongly implicated in the pathogenesis of diabetes and Alzheimer's disease. We recently developed the first effective inhibitors of IDE, peptide hydroxamates that, while highly potent and selective, are relatively large (MW >740) and difficult to synthesize. We present here a facile synthetic route that yields enantiomerically pure derivatives comparable in potency to the parent compounds. Through the generation of truncated variants, we identified a compound with significantly reduced size (MW = 455.5) that nonetheless retains good potency (k_i = 78 ± 11 nM) and selectivity for IDE. Notably, the potency of these inhibitors was found to vary as much as 60-fold in a substrate-specific manner, an unexpected finding for active-site directed inhibitors. Collectively, our findings demonstrate that potent, small-molecule IDE inhibitors can be developed that, in certain instances, can be highly substrate selective.

Keywords

insulin-degrading enzyme; diabetes melittus; Alzheimer disease; protease inhibitors; hydroxamic acids

Introduction

Insulin-degrading enzyme (IDE) is a structurally distinctive zinc-metalloprotease responsible for catabolizing insulin, the amyloid ß-protein (Aß) and other intermediate-sized peptide substrates[1]. IDE is strongly implicated in the pathogenesis of multiple highly prevalent diseases, including type 2 diabetes melittus (T2DM), Alzheimer's disease, and varicella zoster virus infection[2–4]. Despite its clear biological significance, elucidation of IDE's role in these disorders, as well as its fundamental role in regulating insulin signaling[5], has been hindered by the lack of suitable pharmacological inhibitors. Moreover, considerable evidence suggests that IDE inhibitors may hold therapeutic value, particularly for T2DM and other disorders involving impaired insulin signaling[2, 6].

[*]To whom correspondence should be addressed. Phone: 904-254-3050. Fax: 904-953-6276., Leissring@mayo.edu.

IDE possesses a highly distinctive "clamshell"-like structure, consisting of two bowl-shaped halves (IDE-N and IDE-C), which are connected by a flexible linker, allowing the protease to transition between "closed" and "open" conformations[1]. In the closed conformation the two halves encapsulate a large (~13,000 Å^3) internal chamber[1]. The active site of IDE is bipartite, being made up of residues in both the IDE-N and IDE-C domains, and is only fully formed when the protease is in the closed conformation[7].

Using a substrate-based, rational design approach, we recently developed conventional and retro-inverso peptide hydroxamate inhibitors of IDE[8]. These compounds are >10^5-fold more potent than previously described inhibitors and, despite their relatively primitive design, show remarkable selectivity for IDE vis-a-vis other zinc-metalloproteases (~10^4-fold). Despite these merits, as relatively large (MW >740), peptidic compounds that are difficult to synthesize, these inhibitors are less than ideal as chemical probes or pharmacophores for future drug development.

To address these limitations, we describe here the synthesis and characterization of multiple variants of our original, 4-residue peptide hydroxamate IDE inhibitors, including variants developed via a facile alternative synthetic route. Using an IDE-inhibitor co-crystal structure as a guide, we focused on the effects of truncation, modification of the P_2' residue, and variation of the terminal group. Among other advances, we describe a novel variant that is considerably smaller than the parent compound (MW = 455.5) that nonetheless exhibits good potency ($k_i = 87 \pm 11$ nM). Through subsequent characterization of a diverse set of conventional and retro-inverso peptide hydroxamates, we discovered that the potency of certain compounds varies dramatically in a substrate-dependent manner, a highly unexpected finding for active site-directed inhibitors. To account for this unusual property, we propose a novel model wherein interactions among the enzyme, substrate, and inhibitor act in concert to determine the effective potency of inhibition. The insights gained from this study may facilitate the eventual development of more drug-like IDE inhibitors, including substrate-selective compounds.

Results

Previously, we used a substrate-based, rational-design approach[9] to develop peptide hydroxamate inhibitors of IDE (Figure 1A)[8]. Optimization by incorporation of 2-naphthylalanine (2Nap) at the P_1' position yielded the highly potent ($k_i = 2.96 \pm 0.20$ nM), 4-residue conventional peptide hydroxamate, IDE inhibitor 1, (Ii1, **1a,** Figure 1B). We also generated the corresponding retro-inverso peptide hydroxamate **2** (Figure 1C), that, though less potent ($k_i = 78 \pm 4.2$ nM), had the advantage of being readily synthesized by solid-phase peptide synthesis (SPPS) from commercially available components[8].

The co-crystal structure of inhibitor **1a** bound to human IDE was subsequently determined at 2.6-Å resolution[8] (Figure 1D), revealing several salient features informing the present study. First, the positioning of the P_3' and P_4' residues was not resolvable from the co-crystal structure, and these residues were instead predicted to protrude into the internal chamber of IDE. Analysis of the cleavage-site specificity of IDE also showed no preference for specific residues at these positions. Together, these results suggest that the P_3' and P_4' residues might

be dispensable for effective IDE inhibition. Second, inhibitor **1a** makes extensive contacts not only with IDE-N, which contains the residues involved in zinc-binding and catalysis, but also with IDE-C, portions of which make up the second half of IDE's bipartite active site[7]. This configuration suggests that inhibitor **1a** exerts its inhibitory effect by maintaining IDE in the "closed" conformation. Third, the latter feature appeared to be mediated in part by the guanidinium functionality of the P_2' Arg residue, which appears well positioned to interact electrostatically with Glu817 within IDE-C. Nevertheless, this interaction is not direct but is instead mediated via an intervening water molecule, suggesting it might be strengthened by extending the linker joining the guanidinium functionality to the peptide backbone.

Although the bulk of inhibitor **1a** is simply a conventional peptide, synthesis of the 2Nap-containing P_1' precursor in enantiomerically pure form is cumbersome, requiring a complex, multi-step synthesis with a relatively poor yield[8]. We therefore tested an alternative synthetic route, following Cravatt and colleagues[10], wherein the P_1' residue and hydroxamate functionality are generated from ketal-based precursors **7a** or **7b** (Scheme 1), which can in turn be readily attached to peptides generated by SPPS (Scheme 2). This approach results in enantiomerically pure products in comparatively high yield, albeit containing an −OH group attached to the α-carbon adjacent to the hydroxamate in one of two possible orientations (Scheme 2).

Variants of the 4-residue inhibitor **1a** with the α-carbon −OH group in the S and R orientation (inhibitors **8a** and **8b**, respectively) exhibited k_i values of 25.9 ± 1.2 and 103 ± 6.9 nM, respectively (Table 1), using a well-characterized assay involving the fluorogenic peptide substrate, FRET1[11]. Although inhibitors **8a** and **8b** were less potent than the parent inhibitor **1a**, their ease of synthesis represents a distinct advantage so derivatives of these compounds were included in subsequent SAR studies.

Based on the observation that IDE lacks preferences for specific amino acids at the P_3' and P_4' positions (Figure 1A), together with the findings that these residues were poorly resolved in the inhibitor **1a**:IDE co-crystal structure, with the peptide backbone projecting into the internal chamber (Figure 1D), we investigated whether these residues were not essential for potent inhibition of IDE. To that end, we generated truncated forms of inhibitors **1a**, **8a** and **8b** lacking one or both of these residues. The synthetic route used to generate variants of inhibitor **1a** (Scheme 3) yields products with the 2Nap residue in both the S and R orientations, so diastereomers of both orientations were generated and characterized. The truncated, 2-residue variant of inhibitor **1a**—inhibitor **9a**—exhibited dramatically poorer potency ($k_i = 1.15 \pm 0.38$ μM). Consistent with previous results[8], the variant of inhibitor **1a** containing 2Nap in the S orientation, inhibitor **1b**, was significantly less potent than the parent molecule ($k_i = 73.3 \pm 4.2$ nM). This pattern held for the corresponding 2-residue variant, inhibitor **9b**, which was found to be inactive. Truncation of inhibitors **8a** and **8b**, containing the α-carbon −OH functionality in the S and R orientation, respectively, resulted in a similar diminution of potency (Table 2). Of note, the 2-residue variant of inhibitor **8a**, inhibitor **11a**, was unexpectedly found to be *more* potent ($k_i = 7.75 \pm 1.6$ μM) than the 3-residue version, inhibitor **10a** ($k_i = 18 \pm 1.1$ μM). By contrast, 3- and 2-residue versions of inhibitor **7b** (inhibitors **10b** and **11b**, respectively) exhibited potencies that decreased in proportion to the degree of truncation ($k_i = 498 \pm 10$ nM and 7.02 ± 0.33 μM, respectively).

The inhibitor **1a**:IDE co-crystal structure (Figure 1E) suggests that the P_2' Arg residue makes a potentially key interaction with Glu817, which we hypothesized might be further optimized by extending the linker between the guanidinium group and the peptide backbone. To test this, we generated variants of inhibitors **9a**, **9b** and **11a** containing homoArg in the place of Arg (inhibitors **12a**, **12b** and **13**, respectively). Rather than improving potency, this modification was found instead to abolish activity (Table 3). To investigate possible reasons for this, we conducted computational docking of inhibitor **9a** with the crystal structure of IDE (see Experimental Section). In the top-scoring poses, the longer linker in homoArg unexpectedly permitted the guanidinium functionality to interact with Ser138, resulting, in turn, in the displacement of the P_1' 2Nap residue from the S_1' pocket (Figure 2). Thus, rather than promoting electrostatic interactions between the guanidinium and Glu817, as hypothesized, the longer linker in homoArg appears to promote alternative, non-optimal binding modes.

Synthesis of inhibitors **9a** and **9b** involved the generation of 2-residue intermediates containing a C-terminal O-allyl moiety as an orthogonal protecting group (inhibitors **14a** and **14b**, Scheme 3). When these were tested for activity, inhibitor **14a** was found to unexpectedly potent ($k_i = 87 \pm 11$ nM), being ~13-fold more potent than the parent amide, **9a**. Overall, inhibitor **14a** proved to be the most potent of all the 2-residue IDE inhibitors investigated in this study. Given its relatively small size (MW = 455.5) and other properties, inhibitor **14a** comprises the most drug-like inhibitor yet described for IDE.

As mentioned, inhibitor **1a** was shown previously to be highly selective ($>10^4$-fold) for IDE vis-à-vis diverse set of zinc-metalloproteases[8]. To assess whether this property was adversely affected by the modifications described above, we tested the most potent variants —inhibitors **8a**, **8b** and **14a**—against a diverse set of zinc-metalloproteases (Figure 3), including neprilysin (NEP), endothelin-converting enzyme-1 (ECE1), ACE, and MMP-2 and -7. We note that all these experiments were conducted using a common substrate (OmniMMP, see Experimental Section). Compared to the parent compound, inhibitor **1a** (Figure 3A), the next most potent derivative, inhibitor **8a,** exhibited considerably poorer selectivity for IDE (Figure 3B), for example, being a relatively effective inhibitor of MMP7 ($IC_{50} = 1.15 \pm 0.32$ μM). By contrast, the less potent diastereomer, inhibitor **8b**, exhibited excellent selectivity for IDE (Figure 3C), exhibiting no or only partial inhibition of any of the other proteases tested at concentrations up to 10 μM. Inhibitor **14a** also showed reasonably good selectivity (Figure 3D), being >100-fold more potent against IDE vis-à-vis the other proteases tested.

In previous work[8], we developed retro-inverso peptide hydroxamate inhibitors of IDE. Although such compounds are, generally speaking, considerably less potent than the corresponding conventional peptide hydroxamates (*c.f.*, inhibitors **1a** and **2**, Figure 1B,C), they can be synthesized with facility by SPPS, with some variants showing excellent potency[8]. Through the testing of a number of retro-inverso inhibitors, we identified a diverse set of compounds exhibiting good potency in our FRET1 activity assay (Table 4), including: a retro-inverso version of inhibitor **1a** with a free amino terminus (inhibitor **15**; $k_i = 49.8 \pm 3.7$ nM); a variant of the latter with Tyr substituted for Trp at the P_3' position (inhibitor **16**; $k_i = 85.1 \pm 5.0$ nM); a previously described inhibitor (ML1-XF)[8] containing Bpa at the

P_2' position, Tyr at the P_3' position, and Glu(EDANS) at the P_4' position (inhibitor **17**; k_i = 43.7 ± 8.0 nM); and a cyclized retro-inverso peptide hydroxamate (inhibitor **18**; k_i = 23.1 ± 1.2 nM). With the exception of inhibitor **18**, these retro-inverso peptide hydroxamates were developed and characterized previously[8].

The latter compounds, together with the most potent conventional peptide hydroxamates (inhibitors **1a**, **8a**, **8b** and **14a**), were subsequently tested using well-characterized assays for Aß[12] and insulin[7] degradation. Consistent with previous findings[8], inhibitor **1a** exhibited apparent k_i (k_i^{app}) values for Aß and insulin degradation that were ~10-fold higher than for FRET1, a trend that was maintained for most of the 8 compounds tested (Table 5, Figure 4). However, retro-inverso peptide hydroxamates **15** and **17** were found to deviate significantly from this pattern. Inhibitor **15** exhibited a k_i^{app} value for insulin degradation that was >60-fold higher than that obtained with the FRET1 degradation assay, while showing no appreciable difference with the Aß degradation assay (Table 5, Figure 4). Conversely, inhibitor **17** exhibited a k_i^{app} value >30-fold *lower* for Aß degradation relative to the k_i for FRET1 degradation and ~300-fold lower relative to that for insulin degradation (Table 5, Figure 4).

Discussion and conclusions

Since its discovery in 1949[13], IDE has been considered to be an attractive therapeutic target for the treatment of T2DM and other disorders involving impaired insulin signaling[6]. Supporting the merits of this approach, a purified endogenous inhibitor of IDE (non-proteinaceous, but of undetermined identity), was shown to potentiate and prolong the hypoglycemic effect of insulin in vivo as early as 1955[14]. Nevertheless, despite widespread interest in their development throughout the 1950s, effective inhibitors of IDE did not emerge for more than a half-century[8].

Our group has pursued the development of effective IDE inhibitors for more than a decade[15]. After failing to identify effective inhibitors through high-throughput screening of small-molecule compound libraries[8], we employed a classical rational design approach, wherein the preferred cleavage-site specificity of IDE was determined de novo[9] and used to design peptide hydroxamic acids[8]. Following optimization of the P_1' position, these efforts yielded inhibitor **1a** (Ii1), a compound with excellent potency (k_i = 2.96 ± 0.20 nM) and unexpectedly good selectivity (~10^4-fold) vis-à-vis other zinc-metalloproteases and representative member of other protease classes[8]. In the present study, we sought to further optimize inhibitor **1a**, focusing in particular on its principal limitations, including its cumbersome route of synthesis and its relatively large size, with the ultimate goal of developing derivatives amenable to conversion to non-peptidic inhibitors with drug-like properties.

To circumvent the complex synthesis of inhibitor **1a**, variants derived from ketal-based P_1' precursors **7a** and **7b** were developed and characterized. The resulting 4-residue compounds (inhibitors **8a** and **78**), which differ from the parent compound only by the inclusion of an −OH group on the α-carbon between the hydroxamate and the peptide backbone, were much more tractable to synthesize, and yielded enantiomerically pure products in significantly

higher yield, but were ~9- and ~35-fold less potent than inhibitor **1a**, depending on the orientation of the α-carbon –OH group (S and R, respectively). Nevertheless, given that inhibitor **8a** retains low-nanomolar potency (k_i = 25.9 ± 1.2 nM) and, in particular, is readily synthesized in high yield, we consider inhibitor **8a** to be a significant improvement over inhibitor **1a**. Despite its relatively poorer potency, our analysis suggests that inhibitor **8b** may in fact be superior to inhibitor **8a** in terms of selectivity for IDE.

The relatively large size of inhibitor **1a** (MW = 743.8) was the second limitation we sought to optimize. Based on the inhibitor **1a**:IDE co-crystal structure and other considerations, we hypothesized that the P_4' and/or P_3' redidues in inhibitor **1a** might be dispensable. N truncated versions of inhibitors **1a**, **8a** and **8b** were, in general, found to be far less potent than the parent molecules. On the other hand, inhibitor **14a**, a 2-residue variant of inhibitor **1a** containing a C-terminal O-allyl group, was found to exhibit good potency (k_i = 87 ± 11 nM). These results suggest that the P_3' and P_4' residues of latter inhibitors do in fact interact substantially with the active site of IDE, although—as is evident from the lack of resolution of these moieties in the inhibitor **1a**:IDE co-crystal structure, together with the lack of cleavage-site specificity at these positions[8]—not merely via a single mode of binding. Molecular docking of inhibitor **14a** was performed (see Experimental Section), but this approach failed to identify interactions between the O-allyl moiety and specific residues within IDE of sufficient strength to account for the increased potency of this compound, suggesting that multiple binding modes are likely operative in this instance, as well. Whatever the precise mechanism(s), our findings suggest that the P_3' and P_4' residues are not strictly required to achieve potent inhibition, a result that augurs well for the eventual development of effective small-molecule (MW = <500) IDE inhibitors. Given its small size, its potency, and its selectivity for IDE, inhibitor **14a** constitutes an excellent pharmacophore for future drug development.

A key insight emerging from the inhibitor **1a**:IDE co-crystal structure was the finding that the inhibitor makes extensive contacts with both halves of IDE's active site, evidently acting like a "latch" to maintain the protease in the closed conformation. In an attempt to optimize these interactions, we hypothesized that the P_2' Arg residue could be modified to interact more strongly with Glu817 within IDE-C by extending the linker between the guanidinium moiety and the peptide backbone. We tested this by incorporating homoArg into 2-residue conventional peptide hydroxamates (inhibitors **12a**, **12b** and **13**). Contrary to expectations, this modification actually resulted in substantial decreases in potency relative to the parent compounds. Subsequent analysis by computational docking suggests that longer alkane linker in homoArg permits multiple sub-optimal modes of binding, in part by increasing the flexibility of the linker. It remains possible that incorporation of homoArg into 3- or 4-residue hydroxamates might help to overcome these alternate binding modes, and favor interaction with Glu817, by limiting the range of motion of the P_2' residue. However, in light of the substantially diminished potency of most 3- and 2-residue inhibitors, de novo optimization of the P_2' residue in 2-residue inhibitors (e.g., inhibitor **14a**) might be a more fruitful route to improving potency. In this connection, we note that Bpa was well tolerated at the P_2' position (e.g., inhibitor **17**) in retro-inverso peptide hydroxamates, suggesting that

relatively large residues can be tolerated at this position, a feature that might permit more substantial interactions with the C-terminal half of IDE's active site.

One of the more notable aspects of the current study was the discovery that the potency of individual inhibitors, though all presumably interacting with the active-site zinc, varied substantially in a substrate-dependent manner. We observed both increases and decreases in potency, depending on the particular inhibitor and the particular substrate tested. Substrate-dependent pharmacologal modulation has been observed in multiple contexts previously. For example, ATP inhibits the degradation of insulin[16] and Aß[11], yet profoundly activates the degradation of FRET1[11] or other short fluorogenic substrates[17]. Unrelated drug-like compounds have also been identified that exhibit comparable effects[11]. Conversely, Çakir and colleagues used computational methods to identify compounds interacting with IDE's exosite that are reported to activate insulin degradation[18]. Although these unusual properties are undoubtedly attributable to the many novel structural features of IDE—including its bipartite active site and the fact that the substrate and inhibitors can both be contained within the internal chamber—it is nevertheless difficult to postulate a definitive model that cleanly accounts for all of the reported effects.

In sum, this study made considerable progress in optimizing the first effective inhibitor of IDE, inhibitor **1a**. We developed variants that are more tractable to synthesize, and also identified truncated versions that retain good potency while being considerably smaller in size and retaining good selectivity for IDE. In addition, we demonstrate that active site-directed compounds can inhibit IDE in a highly substrate-selective manner. Collectively, these findings are expected to facilitate the development of drug-like IDE inhibitors suitable for a variety of experimental and medicinal applications.

Experimental Section

Synthesis of 1a and 1b

Inhibitors **1a** and **1b** were synthesized, purified and characterized in a previous publication[8].

Synthesis of ketal-based P$_1$' precursors 7a and 7b.

(2*S*,3*R*)-Diisopropyl 2-hydroxy-3-(naphthalen-2-ylmethyl)succinate

(5): Diisopropyl-2*S*-hydroxybutanedioate (**3**) (5.00 g, 22.91 mmol) was added dropwise to a solution of 1M LDA (2.5 eq) in THF maintained at the temperature at −70 °C. After the addition the reaction mixture was slowly warmed to −15° C and stirred for 8 h (CCl$_4$-dry ice). The reaction mixture was then cooled to −70 °C and 2-naphthylmethyl bromide (**4**) (5.57 g, 25.2 mmol) dissolved in THF (5 mL) was added slowly, ensuring that the temperature did not exceeded −65° C. The mixture was warmed to −40 °C (ACN-dry ice bath) and stirred for 18 h before quenching at −15 °C with citric acid. The organic layer was separated, washed with 10% NaHCO$_3$ (50 mL) and brine (30 mL), then dried over MgSO$_4$, filtered and concentrated. The crude product was purified over flash chromatography using 5-15% ethyl acetate/hexane as eluent, affording the product as bright yellow oil (3.50 g, 43%). ^{1}H NMR (300 MHz, CDCl$_3$): δ 1.13-1.48 (m, 12H), 3.05-3.23 (m, 1H), 3.27-3.37 (m,

2H), 4.09 (dd, 1H, J = 2.9, 5.3 Hz), 4.94-5.13 (m, 2H), 7.39-7.48 (m, 3H), 7.73-7.82 (m, 4H). MS m/z (ESI) 380.90 (M+Na)$^+$.

(2S,3R)-2-hydroxy-3-(naphthalen-2-ylmethyl)succinic acid (6): (2S,3R)-Diisopropyl 2-hydroxy-3-(naphthalen-2-ylmethyl)succinate (**5**) (3.25 g, 9.07 mmol) was dissolved in dioxane (7 mL) and water (7 mL), and a solution of KOH (2.035 g, 36.30 mmol) in water (11 mL) was added and the mixture was heated at 90 °C overnight. The solution was then allowed to cool at room temperature and then treated with an ion exchange resin (Dowex 50X4-400, 100 mL), filtered and washed with methanol. The filtrate was evaporated under reduced pressure to yield the title compound as yellow gummy sold (2.462 g, 99%). ^{1}H NMR (300 MHz, CDCl$_3$): δ 3.17-3.47 (m, 3H), 4.13 (d, 1H, J = 2.3 Hz), 7.39-7.50 (m, 3H), 7.75-7.84 (m, 4H). MS m/z (ESI) 272.76 (M-1)$^+$.

(R)-2-((S)-2,2-Dimethyl-5-oxo-1,3-dioxolan-4-yl)-3-(naphthalen-2-yl)propanoic acid (7a): ((2S,3R)-2-Hydroxy-3-(naphthalen-2-ylmethyl)succinic acid (1.88 g, 6.85 mmol) was dissolved in dimethoxypropane (70 mL) and DMF (10 mL) and p-toulenesulfonic acid (0.354 g, 2.056 mmol) was added. The reaction mixture was stirred overnight at 40° C overnight. The solvents were then removed under reduced pressure. The residue was dissolved in ether and the organic solution was washed with water and brine, and dried over MgSO$_4$. After filtration and evaporation, the product was obtained as a brownish solid (1.46 g, 68%). ^{1}H NMR (300 MHz, CDCl$_3$): δ 1.50 (s, 3H), 1.62 (s, 3H), 3.15 (dd, 1H, J = 9.3, 13.2 Hz), 3.36-3.40 (m, 1H), 3.48 (dd, 1H, J = 5.9, 13.2 Hz), 4.32 (d, 1H, J = 3.4 Hz), 7.36 (dd, 1H, J = 1.5, 8.4 Hz), 7.42-7.50 (m, 2H), 7.70 (s, 1H), 7.78-7.83 (m, 3H). ^{13}C NMR (125 MHz, DMSO) 25.8, 26.3, 33.7, 47.8, 73.2, 110.6, 125.6, 126.1, 127.3, 127.4, 127.5, 127.5, 128.0, 131.9, 133.1, 136.3, 171.7, 171.8. HR ESI-MS [M+H]+ m/z = 315.1239 (calc. for C$_{18}$H$_{19}$O$_5$: 315.1232)

(R)-2-((R)-2,2-Dimethyl-5-oxo-1,3-dioxolan-4-yl)-3-(naphthalen-2-yl)propanoic acid (7b): This compound was synthesized following the procedure described for compound **7a**, starting with diisopropyl-2R-hydroxybutanedioate and procecing via purification of the appropriate diasteromer of **5** ((2R,3R)-Diisopropyl 2-hydroxy-3-(naphthalen-2-ylmethyl)succinate). ^{1}H NMR (500 MHz, DMSO): δ 1.50 (s, 3H), 1.57 (s, 3H), 3.03 (m, 1H), 3.30-3.36 (m, 2H), 4.53 (d, 1H, J = 3.1 Hz), 7.42-7.52 (m, 3H), 7.77 (s, 1H), 7.84-7.90 (m, 3H), 12.82 (brs, 1H). ^{13}C NMR (125 MHz, DMSO) 25.7, 26.3, 32.7, 48.5, 73.4, 110.5, 125.6, 126.1, 127.1, 127.3, 127.4, 127.5, 127.9, 131.9, 133.0, 136.1, 171.8, 173.1. HR ESI-MS [M+H]+ m/z = 315.1227 (calc. for C$_{18}$H$_{19}$O$_5$: 315.1232).

Synthesis of peptide hydroxamates by SPPS from ketal-based P$_1$' precursors 7a and 7b.

General procedure.—Rink amide resin (Chem-impex international) (403 mg, 0.65 mmol/g of Fmoc-blocked amino groups) was placed in a clamped glass filter funnel with a glass frit. A slow, steady flow of dry nitrogen was allowed to pass through the resin from the lower end via a piece of Tygon tubing. The resin was swollen with DCM for 30 min, then drained. Resin swelling procedure was repeated for 10 min. After draining, the resin was washed with DMF (10 mL x 4). Fmoc on the Rink amide resin was removed by shaking with 10 ml of 20% piperidine (PIP) in dimethylformamide (DMF) under dry nitrogen for

15 min and the liquid phase drained. This process was repeated once. After washing the deprotected resin with DMF (10 mL x 5), the first Fmoc-amino acid was coupled to the resin by addition of a clear preformed reagent cocktail prepared by vortexing a mixture of 2.2 ml of *O*-(7-azabenzotriazol-1-yl)-*N*,*N*,*N'*,*N'*-tetramethyluronium hexafluorophosphate (HATU), DIPEA (1.0 mmol each) in DMF, and solid Fmoc (*t*Bu)-protected amino acid (1.00 mmol). The resulting suspension was shaken under nitrogen for 1 h at room temperature. Completion of the coupling reaction was monitored by Kaiser test. The coupling was repeated as needed. After ensuring the coupling reaction, the liquid residue was drained off with nitrogen pressure and the resin was washed with dry DMF (10 ml x 4). The Fmoc amine protecting group on the newly added amino acid was removed with 20% PIP as described above. This process of Fmoc removal and coupling was repeated with the remaining Fmoc (Boc) or (Pbf)-protected amino acids and in the peptide sequence. After final coupling with (*R*)-2-((*S*)-2,2-dimethyl-5-oxo-1,3-dioxolan-4-yl)-3-(naphthalen-2-yl)propanoic acid or its enantiomer and thorough washing with DMF (10 mL x 3), the resin was treated with $NH_2OH \cdot HCl$ (40 mmol) and of DIPEA (80 mmol) in DMF (2 mL) and heated at 50° C under nitrogen over night. The solvent was removed by filtration and the residue was washed sequentially with ethanol and with dichloromethane (DCM) (10 ml x 4). Finally, the resin-bound (*t*Bu)-, (Boc)- and Pbf-protected peptide was cleaved off the resin by wrist action shaking for 2h with 10 ml of 2.5% triisopropyl silane, 2.5% H_2O in trifluoroacetic acid (TFA) under nitrogen. After final draining of the cleaved peptide solution, the resin was thoroughly washed with DCM (10 ml x 4). The extracts and the DCM washes were combined. The volatiles were removed under rotary evaporation to afford the crude peptide. Dry diethyl ether was added and the resulting precipitate was removed by centrifugation and dried under high vacuum. The peptide in the crude residue was purified by reverse-phase HPLC using a linear of acetonitrile:water gradient containing 0.1% TFA. Compounds **8a**, **8b**, **10a**, **10b**, **11a**, **11b**, and **13** were synthesized by following this general procedure.

(*S*)-5-Amino-4-((*S*)-2-((*S*)-5-guanidino-2-((2*R*,3*S*)-3-hydroxy-4-(hydroxyamino)-2-(naphthalen-2-ylmethyl)-4-oxobutanamido)pentanamido)-3-(1*H*-indol-2-yl)propanamido)-5-oxopentanoic acid (8a):

(Yield: 89 mg, 80%) ^1H NMR (300 MHz, CD_3OD): δ 1.19-1.31 (m, 2H), 1.33-1.44 (m, 1H), 1.56-1.79 (m, 2H), 1.91-2.02 (m, 1H), 2.15 (t, 2H, *J* = 7.6 Hz), 2.86-2.97 (m, 4H), 3.02-3.09 (m, 2H), 4.02 (d, 1H, *J* = 4.8 Hz), 4.13-4.20 (m, 2H), 4.35-4.39 (m, 1H), 6.90-7.01 (m, 3H), 7.19-7.34 (m, 4H), 7.46 (d, 1H, *J* = 7.4 Hz), 7.58-7.67 (m, 4H), 7.83 (d, 1H, *J* = 7.1 Hz). HR ESI-MS [M+H]+ *m/z* = 760.3441 (calc. for $C_{37}H_{46}N_9O_9$: 760.3418).

(*S*)-5-Amino-4-((*S*)-2-((*S*)-5-guanidino-2-((2*S*,3*R*)-3-hydroxy-4-(hydroxyamino)-2-(naphthalen-2-ylmethyl)-4-oxobutanamido)pentanamido)-3-(1*H*-indol-2-yl)propanamido)-5-oxopentanoic acid (8b):

(Yield: 68 mg, 87%) ^1H NMR (300 MHz, CD_3OD): δ 1.18-1.29 (m, 2H), 1.31-1.41 (m, 1H), 1.52-1.77 (m, 2H), 1.91-2.00 (m, 1H), 2.17 (t, 2H, *J* = 7.7 Hz), 2.81-2.93 (m, 4H), 3.00-3.10 (m, 2H), 4.05 (d, 1H, *J* = 4.7 Hz), 4.15-4.19 (m, 2H), 4.36-4.40 (m, 1H), 6.91-7.02 (m, 3H), 7.18-7.33 (m, 4H), 7.456 (d, 1H, *J* = 7.3 Hz), 7.57-7.66 (m, 4H), 7.82 (d, 1H, *J* = 7.2 Hz). HR ESI-MS [M+H]+ *m/z* = 760.3442 (calc. for $C_{37}H_{46}N_9O_9$: 760.3418).

(2R,3S)-N^1-((S)-1-((S)-1-Amino-3-(1H-indol-2-yl)-1-oxopropan-2-ylamino)-5-guanidino-1-oxopentan-2-yl)-N^4,3-dihydroxy-2-(naphthalen-2-ylmethyl)succinamide (10a): (Yield: 51 mg, 77%) ^{1}H NMR (300 MHz, CD$_3$OD): δ 0.59-0.64 (m, 2H), 1.04-1.11 (m, 1H), 1.31 (s, 2H), 1.40-1.44 (m, 1H), 2.44 (t, 2H, J = 6.9 Hz), 2.98-3.16 (m, 4H), 4.11-4.14 (m, 1H), 4.20 (d, 1H, J = 6.8 Hz). 4.59-4.67 (m, 1H), 6.98-7.11 (m, 3H), 7.30-7.48 (m, 4H), 7.62 (d, 1H, J = 7.7 Hz), 7.66 (s, 1H), 7.76-7.82 (m, 3H), 7.88 (d, 1H, J = 8.7 Hz), 8.07 (d, 1H, J = 7.8 Hz). ^{13}C NMR (125 MHz, DMSO) 24.4, 27.6, 28.1, 34.0, 50.9, 52.0, 53.6, 69.8, 71.2 110.3, 111.2, 118.2, 118.4, 120.8, 123.8, 125.3, 126.0, 126.7, 127.2, 127.3, 127.4, 127.5, 127.7, 131.7, 133.0, 136.0, 136.7, 156.7, 168.4, 170.7, 172.5, 173.5. HR ESI-MS [M+H]+ m/z = 631.3008 (calc. for C$_{32}$H$_{39}$N$_8$O$_6$: 631.2992).

(2S,3R)-N^1-((S)-1-((S)-1-amino-3-(1H-indol-2-yl)-1-oxopropan-2-ylamino)-5-guanidino-1-oxopentan-2-yl)-N^4,3-dihydroxy-2-(naphthalen-2-ylmethyl)succinamide (10b): (Yield: 90 mg, 85%) ^{1}H NMR (300 MHz, CD$_3$OD): δ 0.61-0.66 (m, 2H), 1.06-1.13 (m, 1H), 1.33 (s, 2H), 1.41-1.46 (m, 1H), 2.43 (t, 2H, J = 6.8 Hz), 2.99-3.15 (m, 4H), 4.13-4.17 (m, 1H), 4.22 (d, 1H, J = 6.8 Hz). 4.60-4.68 (m, 1H), 6.99-7.12 (m, 3H), 7.33-7.49 (m, 4H), 7.63 (d, 1H, J = 7.6 Hz), 7.65 (s, 1H), 7.75-7.81 (m, 3H), 7.88 (d, 1H, J = 8.6 Hz), 8.05 (d, 1H, J = 7.7 Hz). HR ESI-MS [M+H]+ m/z = 631.3007 (calc. for C$_{32}$H$_{39}$N$_8$O$_6$: 631.2992).

(2R,3S)-N^1-((S)-1-Amino-5-guanidino-1-oxopentan-2-yl)-N^4,3-dihydroxy-2-(naphthalen-2-ylmethyl)succinamide (11a): (Yield: 69 mg, 88%) ^{1}H NMR (300 MHz, CD$_3$OD): δ 1.56 (br s, 3H), 1.84 (br s, 1H), 3.11 (br s, 5H), 4.29 (br s, 1H), 7.24-7.83 (m, 3H), 7.72 (s, 1H), 7.78-7.83 (m, 3H). ^{13}C NMR (125 MHz, DMSO) 24.8, 28.7, 34.1, 40.3, 50.3, 52.1, 69.7, 125.2, 125.9, 126.7, 127.3, 127.4, 127.5, 127.6, 131.6, 132.9, 136.7, 156.6, 172.0, 173.0. HR ESI-MS [M+H]+ m/z = 445.2208 (calc. for C$_{21}$H$_{29}$N$_6$O$_5$: 445.2199).

(2S,3R)-N^1-((S)-1-amino-5-guanidino-1-oxopentan-2-yl)-N^4,3-dihydroxy-2-(naphthalen-2-ylmethyl)succinamide (11b)—(Yield: 50 mg, 88%) ^{1}H NMR (300 MHz, CD$_3$OD): δ 1.54 (br s, 3H), 1.88 (br s, 1H), 3.13 (br s, 5H), 4.30 (br s, 1H), 7.22-7.84 (m, 3H), 7.71 (s, 1H), 7.79-7.85 (m, 3H). HR ESI-MS [M+H]+ m/z = 445.2210 (calc. for C$_{21}$H$_{29}$N$_6$O$_5$: 445.2199).

(2R,3S)-N^1-((S)-1-amino-6-guanidino-1-oxohexan-2-yl)-N^4,3-dihydroxy-2-(naphthalen-2-ylmethyl)succinamide (13): (Yield: 93 mg, 81%) ^{1}H NMR (300 MHz, CD$_3$OD): δ 1.30-1.36 (m, 2H), 1.44-1.57 (m, 3H), 1.78-1.83 (m, 1H), 3.06-3.24 (m, 5H), 3.99 (s, 1H), 4.16 (d, 1H, J = 4.5 Hz). 4.26-4.30 (m, 1H), 7.42-7.49 (m, 3H), 7.74 (s, 1H), 7.79-7.84 (m, 3H), 8.07 (d, 1H, J = 8.2 Hz). ^{13}C NMR (125 MHz, DMSO) 22.2, 27.9, 31.2, 34.2, 40.6, 50.3 52.2, 70.8, 125.3, 126.0, 126.8, 127.3, 127.4, 127.5, 127.6, 131.7, 133.0, 136.8, 156.8, 168.8, 172.1, 173.4. HR ESI-MS [M+H]+ m/z = 459.2365 (calc. for C$_{22}$H$_{31}$N$_6$O$_5$: 459.2355).

Synthesis of truncated variants of inhibitors 1a and 1b (9a, 9b, 12a, 12b, 14a and 14b).

General procedure.—Compounds **9a**, **9b**, **14a** and **14b** were synthesized by solution phase peptide synthesis using methods described previously[8]. Compounds **12a**, **12b** were synthesized by the same methods used to generate **9a** and **9b**, albeit utilizing homoArg in the place of Arg.

(S)-Allyl5-guanidino-2-((S)-4-(hydroxyamino)-2-(naphthalen-2-ylmethyl)-4-oxobutanamido)pentanoate (14a)—A solution of (6*S*,9*S*)-allyl 1-imino-14,14-dimethyl-9-(naphthalen-2-ylmethyl)-8,11-dioxo-1-(2,2,4,6,7-pentamethyl-2,3-dihydrobenzofuran-5-sulfonamido)-13-oxa-2,7,12-triazapentadecane-6-carboxylate[8] (47.0 mg, 0.064 mmol) in 5% anisole in TFA (6 ml) was stirred at 40° C for 4.5 h. The reaction mixture was cooled and the volatiles were removed in vacuo. The resultant oil was washed with ether (10 mL), dissolved in water (5ml) and filtered. The filtrate was lyophilized to give a crude solid that was further purified by reverse-phase HPLC using a linear 0.1% TFA in acetonitrile:water gradient to give the title compound as a white powder (20.1 mg, 72%). ^{1}H NMR (300 MHz, CD$_3$OD): δ 0.76 (br s, 2H), 1.15-1.42 (m, 2H), 2.17 (dd, 1H, J = 7.4, 14.5 Hz), 2.34 (dd, 1H, J = 7.0, 14.5 Hz), 2.49 (br s, 2H), 2.81 (d, 2H, J = 7.3 Hz) 3.05 - 3.10 (m, 1H), 3.05 (m, 1H), 4.05-4.06 (m, 1H), 4.43 (d, 2H, J = 4.7 Hz), 5.05 (d, 1H, J = 10.4 Hz), 5.15 (d, 1H, J = 17.2 Hz), 5.71-5.80 (m, 1H), 7.22-7.31 (m, 3H), 7.50 (s, 1H), 7.64-7.66 (m, 2H). HR ESI-MS [M+H]+ m/z = 470.2423 (calc. for C$_{24}$H$_{32}$N$_5$O$_5$: 470.2403).

(S)-Allyl5-guanidino-2-((R)-4-(hydroxyamino)-2-(naphthalen-2-ylmethyl)-4-oxobutanamido)pentanoate (14b): This compound was synthesized following the procedure mentioned above (112 mg, 92%. ^{1}H NMR (300 MHz, CD$_3$OD): δ 1.49-1.64 (m, 3H), 1.73-1.75 (m, 1H), 2.13 (dd, 1H, J = 4.2, 14.8 Hz), 2.41 (dd, 1H, J = 10.1, 14.8 Hz), 2.77 (dd, 1H, J = 6.7, 13.1 Hz), 2.88 - 3.06 (m, 3H), 4.14-4.29 (m, 2H), 4.34-4.36 (m, 1H), 4.43 (d, 2H, J = 4.7 Hz), 5.03 (d, 1H, J = 10.5 Hz), 5.08 (d, 1H, J = 18.6 Hz), 5.55-5.68 (m, 1H), 7.26-7.37 (m, 3H), 7.55 (s, 1H), 7.67-7.72 (m, 2H). ^{13}C NMR (125 MHz, DMSO) δ 24.9, 27.9, 33.6, 37.7, 40.3, 42.6, 51.5, 64.7, 117.7, 125.9, 127.0, 127.3, 124.4, 127.6, 131.7, 132.3, 133.0, 136.8, 156.6, 167.6, 171.4, 173.7. HR ESI-MS [M+H]+ m/z = 470.2420 (calc. for C$_{24}$H$_{32}$N$_5$O$_5$: 470.2403).

(S)-*N*^{1}-((S)-1-amino-5-guanidino-1-oxopentan-2-yl)-*N*^{4}-hydroxy-2-(naphthalen-2-ylmethyl)succinamide (9a): (S)-Allyl5-guanidino-2-((S)-4-(hydroxyamino)-2-(naphthalen-2-ylmethyl)-4-oxobutanamido)pentanoate (50.0 mg, 0.064 mmol) was dissolved in 6 M solution anhydrous ammonia in methanol (1.6 mL) at −10° C and stirred under nitrogen at room temperature overnight. The solvent was removed under reduced pressure to afford a white solid (47.0 mg, 99%). ^{1}H NMR (300 MHz, CD$_3$OD): δ 0.56-0.65 (m, 2H), 1.12-1.24 (m 1H), 1.53-1.59 (m, 1H), 2.32 (dd, 1H, J = 3.7, 15.2 Hz), 2.49 (br s, 2H), 2.60 (dd, 1H, J = 10.2, 15.2 Hz), 2.88-2.94 (m, 2H), 3.04-3.07 (m, 1H), 3.96-4.00 (m, 1H), 6.89 (br s, 1H), 7.32-7.43 (m, 3H), 7.59 (s, 1H), 7.73-7.78 (m, 3H), 8.08 (d, 1H, J = 8.0 Hz). ^{13}C NMR (125 MHz, DMSO) 24.7, 28.1, 34.2, 38.3, 40.2, 43.3, 51.9, 125.3, 125.9. 127.0, 127.3, 127.4, 127.5, 127.6, 131.7, 133.0, 136.7, 156.6, 167.9, 173.6, 173.7. HR ESI-MS [M+H]+ m/z = 429.2263 (calc. for C$_{21}$H$_{29}$N$_6$O$_4$: 429.2250).

(R)-N^1-((S)-1-amino-5-guanidino-1-oxopentan-2-yl)-N^4-hydroxy-2-(naphthalen-2-ylmethyl)succinamide (9b).—This compound was synthesized

following the procedure mentioned above (60.2 mg, 97%). ^{1}H NMR (300 MHz, CD$_3$OD): δ 1.53 (m, 3H), 1.79 (br s, 1H), 2.23 (br d, 1H, J = 15.0 Hz), 2.43-.246 (m, 1H), 2.82-2.88 (m, 1H), 2.99-3.07 (m, 4H), 4.25 (br s, 1H), 7.32-7.40 (m, 3H), 7.61 (s, 1H), 7.74-7.76 (m, 3H), 8.08 (d, 1H, J = 7.8 Hz). ^{13}C NMR (125 MHz, DMSO) 24.8, 28.8, 33.7, 37.9, 40.2, 43.0, 51.9, 125.3, 126.0, 127.0, 127.3, 127.4, 127.5, 127.6, 131.7, 133.0, 136.8, 156.6, 167.9, 173.2, 173.4. HR ESI-MS [M+H]+ m/z = 429.2264 (calc. for $C_{21}H_{29}N_6O_4$: 429.2250).

(2R,3S)-N^1-((S)-1-Amino-5-guanidino-1-oxopentan-2-yl)-N^4,3-dihydroxy-2-(naphthalen-2-ylmethyl)succinamide (12a): This compound was synthesized

following the procedure for 9a, albeit substituting homoArg in the place of Arg (69.5 mg, 95%). ^{1}H NMR (300 MHz, CD$_3$OD): δ 1.56 (br s, 3H), 1.84 (br s, 1H), 3.11 (br s, 5H), 4.29 (br s, 1H), 7.24-7.83 (m, 3H), 7.72 (s, 1H), 7.78-7.83 (m, 3H). ^{13}C NMR (125 MHz, DMSO) 24.8, 28.7, 34.1, 40.3, 50.3, 52.1, 69.7, 125.2, 125.9, 126.7, 127.3, 127.4, 127.5, 127.6, 131.6, 132.9, 136.7, 156.6, 172.0, 173.0. HR ESI-MS [M+H]+ m/z = 443.2314 (calc. for $C_{22}H_{31}N_6O_4$: 443.2329).

(2S,3R)-N^1-((S)-1-amino-5-guanidino-1-oxopentan-2-yl)-N^4,3-dihydroxy-2-(naphthalen-2-ylmethyl)succinamide (12b): This compound was synthesized

following the procedure for compound 12a (66.7 mg, 92%).
^{1}H NMR (300 MHz, CD$_3$OD): δ 1.54 (br s, 3H), 1.88 (br s, 1H), 3.13 (br s, 5H), 4.30 (br s, 1H), 7.22-7.84 (m, 3H), 7.71 (s, 1H), 7.79-7.85 (m, 3H). HR ESI-MS [M+H]+ m/z = 443.2318 (calc. for $C_{22}H_{31}N_6O_4$: 443.2329).

Synthesis of retro-inverso peptide hydroxamates (2, 15, 16, 17, 18)

All retro-inverso inhibitors were synthesized by conventional SPPS from commercially available Fmoc-protected amino acids using 2-chlorotrityl hydroxylamine resin, as described[8]. The synthesis, purification and characterization of inhibitors **2, 15**, **16** and **17** is described in a previous publication[8]. Inhibitor **18** was synthesized by a commercial vendor (Anaspec Corp.).

Purification of compounds.

All compounds were purified by reverse-phase HPLC (purity >95%) as described[8].

IDE activity assays

Dose-response determinations for IDE inhibitors were obtained using previously described assays for the degradation of FRET1[11] (5 μM), OmniMMP (5 μM)[8], Aß[12] (200 nM), and insulin[7] (2 nM). All assays were conducted at 22 °C in Assay Buffer (100 mM NaCl, 10 mM MgCl$_2$, 50 mM HEPES, pH 7.4, supplemented with 0.05% BSA) using recombinant human IDE[19]. IC$_{50}$ values were calculated in Prism 5.0 (Graphpad Software, Corp.) then converted to k_i values via the Cheng-Prussoff equation[20] using published k_M values for the different substrates (10.1 μM, 0.82 μM and 71 nM for FRET1[21], Aß[12] and insulin[8], respectively).

Molecular Docking

The starting conformation of ligands was obtained by the method of Polak-Ribière Conjugate Gradient (PRCG) energy minimization with the Optimized Potentials for Liquid Simulations (OPLS) 2005 force field for 5000 steps, or until the energy difference between subsequent structures was less than 0.001 kJ/mol-Å[22]. Our docking methodology has been previously described[23]. Briefly, in order to generate the grids for docking, the ions, molecular refracting molecules 1,4-diethylene dioxide (DIO) were removed from the IDE crystal structure (PDB Code 3E4A)[8]. Inhibitor **1a** was used as the reference ligand to generate the grids. The binding site was generated via multiple overlapping grids with a default rectangular box centered on inhibitor **1a**. Ligands were docked into the catalytic binding site of IDE using Glide extra precision (XP) (Glide, version 5.6, Schrödinger, LLC, New York, NY). Molecular conformations were sampled using previous methods in the literature[24].

We generated XP descriptors to obtain atom-level energy terms such as hydrogen bond interactions, electrostatic interactions, hydrophobic enclosure and pi-pi stacking interactions that resulted during the docking run. The final conformation of the docked ligand was obtained from the optimized, best scoring poses with descriptors of the Glide XP score using a recently developed approach[23,25, 26]. Briefly, we used Phase to automatically generate the pharmacophoric sites (Phase, v3.2, Schrödinger, LLC, New York, NY) using the default set of six chemical features: namely, hydrogen bond acceptor (A), hydrogen bond donor (D), hydrophobic (H), negative ionizable (N), positive ionizable (P), and aromatic ring (R) site. The energetic value assigned to each pharmacophore feature was arrived at as the sum of the Glide XP contributions of the atoms comprising the site. Overall dockings at the active site were quantified and ranked on the basis of these energetic terms[25, 26]. From these features, a common pharmacophore model was developed to evaluate the ability to reproduce known inhibitors using Phase. The distance matching tolerance was set to 2.0 Å. To account for protein flexibility and lessen the effects of minor steric clashes, excluded volumes spheres were created for all receptor atoms within 5 Å around every ligand. Each sphere has a radius corresponding to 50% of the van der Waals radius of the receptor atom. Receptor atoms within 1.5 Å from the ligand were ignored. Figures were generated either using Linux command-line Tachyon, Version 0.99b2, or Tachyon within the Visual Molecular Dynamics (VMD) Version 1.9.1 program[27].

Acknowledgments.

Abbreviations Used:

Aß	amyloid ß-protein
ECE1	endothelin-converting enzyme-1
IDE	insulin-degrading enzyme
IDE-C	IDE C-terminal domain

IDE-N	IDE N-terminal domain
Ii1	IDE inhibitor 1
NEP	neprilysin
SPPS	solid-phase peptide synthesis
T2DM	type 2 diabetes mellitus

References

1. Shen Y; Joachimiak A; Rosner MR; Tang W-J Structures of human insulin-degrading enzyme reveal a new substrate mechanism. Nature 2006, 443, 870–874. [PubMed: 17051221]

2. Abdul-Hay SO; Kang D; McBride M; Li L; Zhao J; Leissring MA Deletion of insulin-degrading enzyme elicits antipodal, age-dependent effects on glucose and insulin tolerance. PLoS ONE 2011, 6, e20818. [PubMed: 21695259]

3. Qiu WQ; Folstein MF Insulin, insulin-degrading enzyme and amyloid-beta peptide in Alzheimer's disease: review and hypothesis. Neurobiol Aging 2006, 27, 190–198. [PubMed: 16399206]

4. Li Q; Ali MA; Cohen JI Insulin degrading enzyme is a cellular receptor mediating varicella-zoster virus infection and cell-to-cell spread. Cell 2006, 127, 305–316. [PubMed: 17055432]

5. Authier F; Posner BI; Bergeron JJ Insulin-degrading enzyme. Clin Invest Med 1996, 19, 149–160. [PubMed: 8724818]

6. Mirsky IA Insulinase, insulinase-inhibitors, and diabetes mellitus. Recent Prog Horm Res 1957, 13, 429–465; discussion 465-471. [PubMed: 13477814]

7. Neant-Fery M; Garcia-Ordonez RD; Logan TP; Selkoe DJ; Li L; Reinstatler L; Leissring MA Molecular basis for the thiol sensitivity of insulin-degrading enzyme. Proc Natl Acad Sci U S A 2008, 105, 9582–9587. [PubMed: 18621727]

8. Leissring MA; Malito E; Hedouin S; Reinstatler L; Abdul-Hay SO; Choudhry S; Fauq AH; Huzarska M; May PS; Choi S; Logan TP; Turk BE; Cantley LC; Manolopoulou M; Tang WJ; Stein RL; Cuny GD; Selkoe DJ Designed inhibitors of insulin-degrading enzyme regulate the catabolism and activity of insulin. PLoS One 2010, 5, e10504. [PubMed: 20498699]

9. Turk BE; Huang LL; Piro ET; Cantley LC Determination of protease cleavage site motifs using mixture-based oriented peptide libraries. Nat Biotechnol 2001, 19, 661–667. [PubMed: 11433279]

10. Saghatelian A; Jessani N; Joseph A; Humphrey M; Cravatt BF Activity-based probes for the proteomic profiling of metalloproteases. Proc Natl Acad Sci U S A 2004, 101, 10000–10005. [PubMed: 15220480]

11. Cabrol C; Huzarska MA; Dinolfo C; Rodriguez MC; Reinstatler L; Ni J; Yeh L-A; Cuny GD; Stein RL; Selkoe DJ; Leissring MA Small-molecule activators of insulin-degrading enzyme discovered through high-throughput compound screening. PLoS ONE 2009, 4, e5274. [PubMed: 19384407]

12. Leissring MA; Lu A; Condron MM; Teplow DB; Stein RL; Farris W; Selkoe DJ Kinetics of amyloid beta-protein degradation determined by novel fluorescence- and fluorescence polarization-based assays. J Biol Chem 2003, 278, 37314–37320. [PubMed: 12867419]

13. Mirsky IA; Broth-Kahn RH The inactivation of insulin by tissue extracts. I. The distribution and properties of insulin inactivating extracts (insulinase). Arch Biochem 1949, 20, 1–9. [PubMed: 18104389]

14. Mirsky IA; Perisutti G Effect of insulinase-inhibitor on hypoglycemic action of insulin. Science 1955, 122, 559–560.

15. Leissring MA; Farris W; Turk BE; Cantley LC; Yeh L; Caclin C; Xing X; Cuny GD; Stein RL; Selkoe DJ Small-molecule inhibitors of insulin-degrading enzyme. Society for Neuroscience Abstract Viewer/Itinerary Planner 2004, Program No. 488.11.

16. Camberos MC; Perez AA; Udrisar DP; Wanderley MI; Cresto JC ATP inhibits insulin-degrading enzyme activity. Exp Biol Med (Maywood) 2001, 226, 334–341. [PubMed: 11368426]

17. Song ES; Juliano MA; Juliano L; Fried MG; Wagner SL; Hersh LB ATP effects on insulin-degrading enzyme are mediated primarily through its triphosphate moiety. J Biol Chem 2004, 279, 54216–54220. [PubMed: 15494400]

18. Cakir B; Dagliyan O; Dagyildiz E; Baris I; Kavakli IH; Kizilel S; Turkay M Structure based discovery of small molecules to regulate the activity of human insulin degrading enzyme. PLoS ONE 2012, 7, e31787. [PubMed: 22355395]

19. Farris W; Leissring MA; Hemming ML; Chang AY; Selkoe DJ Alternative splicing of human insulin-degrading enzyme yields a novel isoform with a decreased ability to degrade insulin and amyloid beta-protein. Biochemistry 2005, 44, 6513–6525. [PubMed: 15850385]

20. Cheng Y; Prusoff WH Relationship between the inhibition constant (K1) and the concentration of inhibitor which causes 50 per cent inhibition (I50) of an enzymatic reaction. Biochem Pharmacol 1973, 22, 3099–3108. [PubMed: 4202581]

21. Song ES; Mukherjee A; Juliano MA; Pyrek JS; Goodman JP Jr.; Juliano L; Hersh LB Analysis of the subsite specificity of rat insulysin using fluorogenic peptide substrates. J Biol Chem 2001, 276, 1152–1155. [PubMed: 11042190]

22. Still WC; Tempczyk A; Hawley RC; Hendrickson T Semianalytical Treatment of Solvation for Molecular Mechanics and Dynamics. Journal of the American Chemical Society 1990, 112, 6127–6129.

23. Caulfield T; Medina-Franco JL Molecular dynamics simulations of human DNA methyltransferase 3B with selective inhibitor nanaomycin A. J Struct Biol 2011, 176, 185–191. [PubMed: 21839172]

24. Caulfield TR; Devkota B Motion of transfer RNA from the A/T state into the A-site using docking and simulations. Proteins 2012.

25. Loving K; Salam NK; Sherman W Energetic analysis of fragment docking and application to structure-based pharmacophore hypothesis generation. J Comput Aided Mol Des 2009, 23, 541–554. [PubMed: 19421721]

26. Salam NK; Nuti R; Sherman W Novel method for generating structure-based pharmacophores using energetic analysis. J Chem Inf Model 2009, 49, 2356–2368. [PubMed: 19761201]

27. Humphrey W; Dalke A; Schulten K VMD: visual molecular dynamics. Journal of molecular graphics 1996, 14, 33–38, 27-38. [PubMed: 8744570]
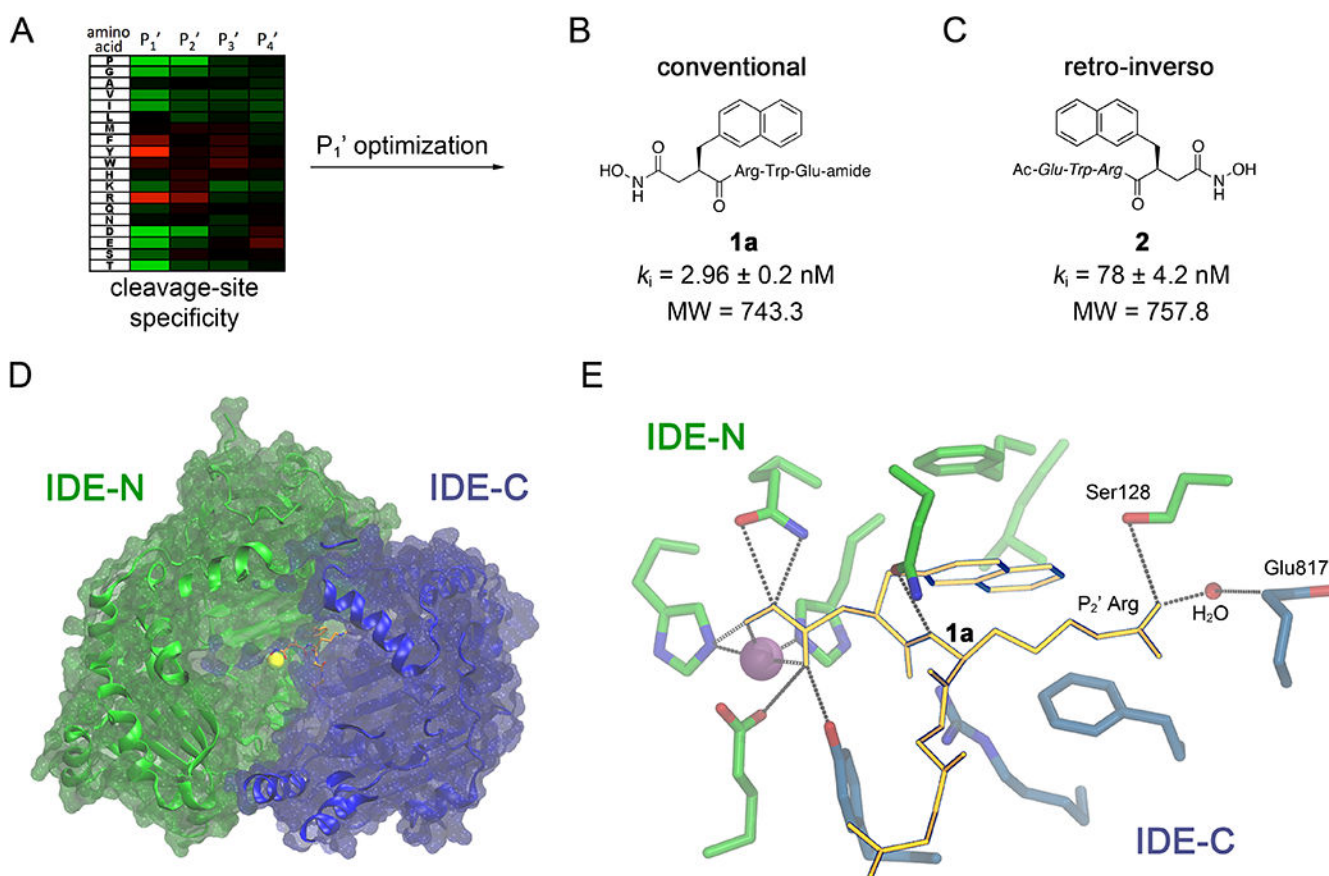
Figure 1.

Development of the first peptide hydroxamate IDE inhibitors and mechanistic insights derived from the inhibitor **1a**:IDE co-crystal structure. *A*, Overview of the rational design approach used to develop peptide hydroxamate inhibitor **1a** (*B*), which involved determination of the cleavage-site specificity (*heat map*) and subsequent optimization of the P_1' position. Note that IDE shows comparatively little preference for specific amino acids at the P_3' and P_4' positions. *B,C*, Conventional (*B*) and retro-inverso (*C*) peptide hydroxamate inhibitors derived from the approach outlined in (*A*). Note that inhibitor **1a** (*B*) is highly potent but relatively large in size. D-amino acids are depicted in *italics*. *D*, The co-crystal structure of inhibitor **1a** (*orange sticks*) bound to a single monomer of human IDE (*blue* and *green ribbons*). Note that inhibitor **1a** is positioned between IDE-N (*green*), which contains the active-site zinc (*yellow sphere*), and IDE-C (*blue*). *E*, Close-up depiction of inhibitor **1a** (*orange sticks*) bound to the active-site of IDE, highlighting the interaction with the zinc atom (*orange sphere*) and residues within IDE-N (*green sticks*) and IDE-C (*blue sticks*). Note that the guanidinium moiety within the P_2' Arg residue makes indirect contact with Glu817 via an intervening water molecule.
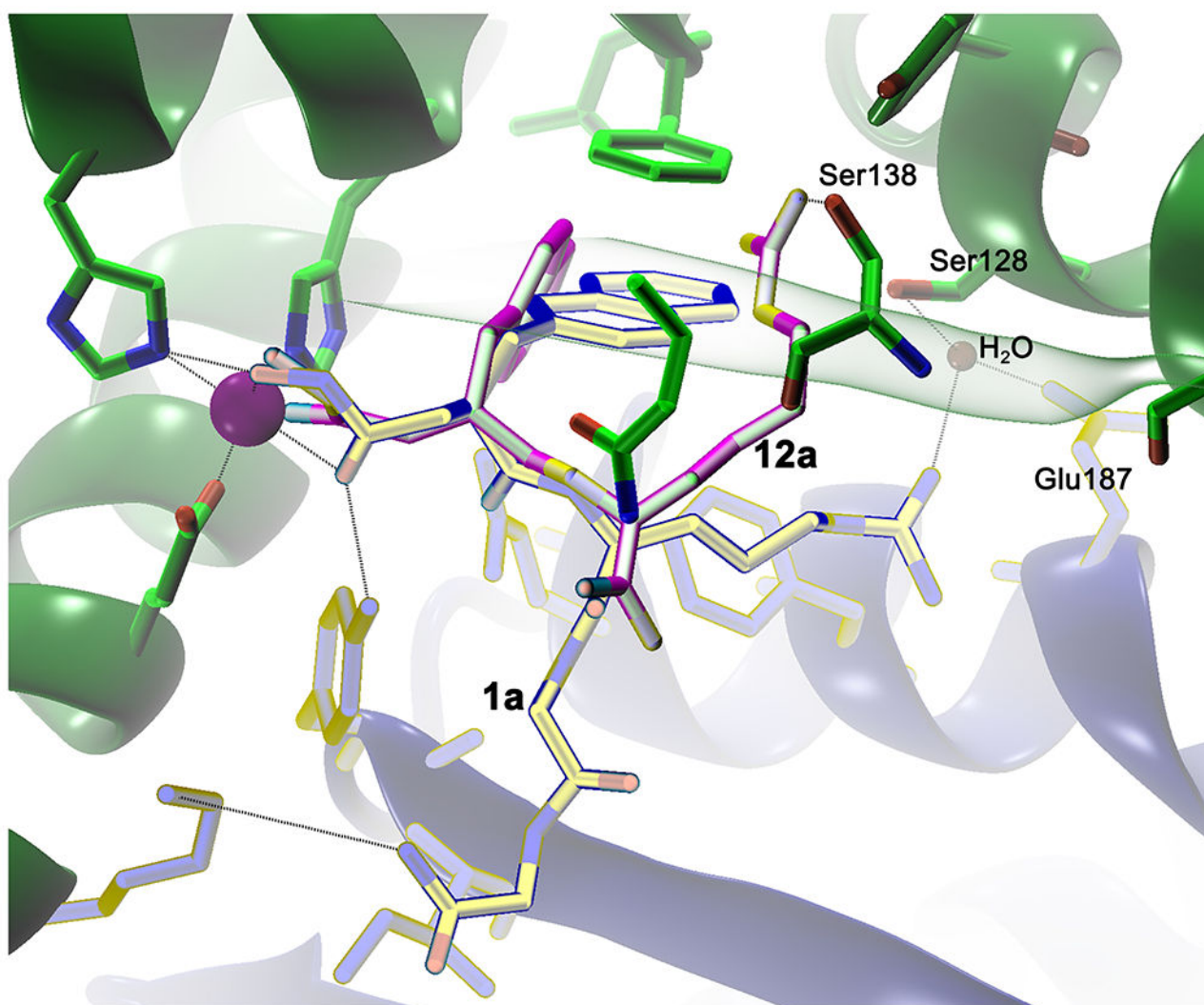
Figure 2.
Computational docking of hydroxamate **12a** suggests why substitution of homoArg for Arg at the P$_2$' position fails to improve potency. Comparison of the lowest energy poses for inhibitor **1a** (*yellow sticks*) versus inhibitor **12a** (*magenta sticks*) bound to the catalytic zinc (*purple sphere*) and residues within IDE-N (*green*) and IDE-C (*blue*). Note that the guanidinium moiety within the homoArg residue of compound **12a** fails to form electrostatic interactions with Glu817, as hypothesized, but instead makes strong contact with Ser138. This alternate interaction appears to force the P$_1$' 2Nap residue into a less stable conformation, while simultaneously reducing the interactions between IDE-N and IDE-C, which are hypothesized to be essential for effective inhibition.
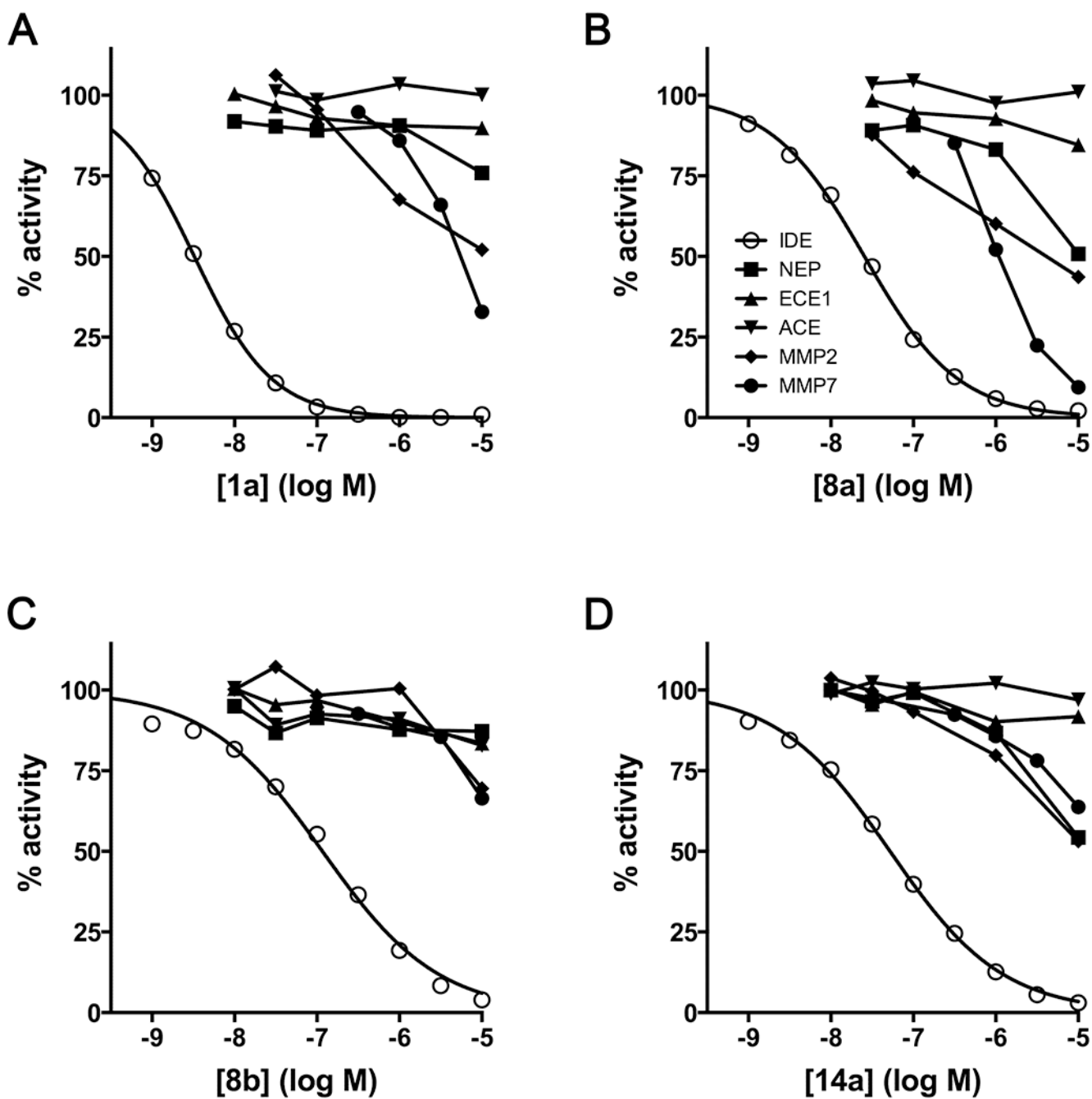
Figure 3.
Conventional peptide hydroxamates show varying degrees of selectivity for IDE. Dose-response curves for inhibitors **1a** (A), **8a** (B), **8b** (C) and **14a** (D) against IDE, NEP, ECE1, ACE, MMP2 and MMP7. The legend in panel B (*inset*) applies to all graphs. Note that MMP7 is rather potently inhibited by inhibitors **1a** and **8a**, but not by inhibitors **8b** or **14a**.
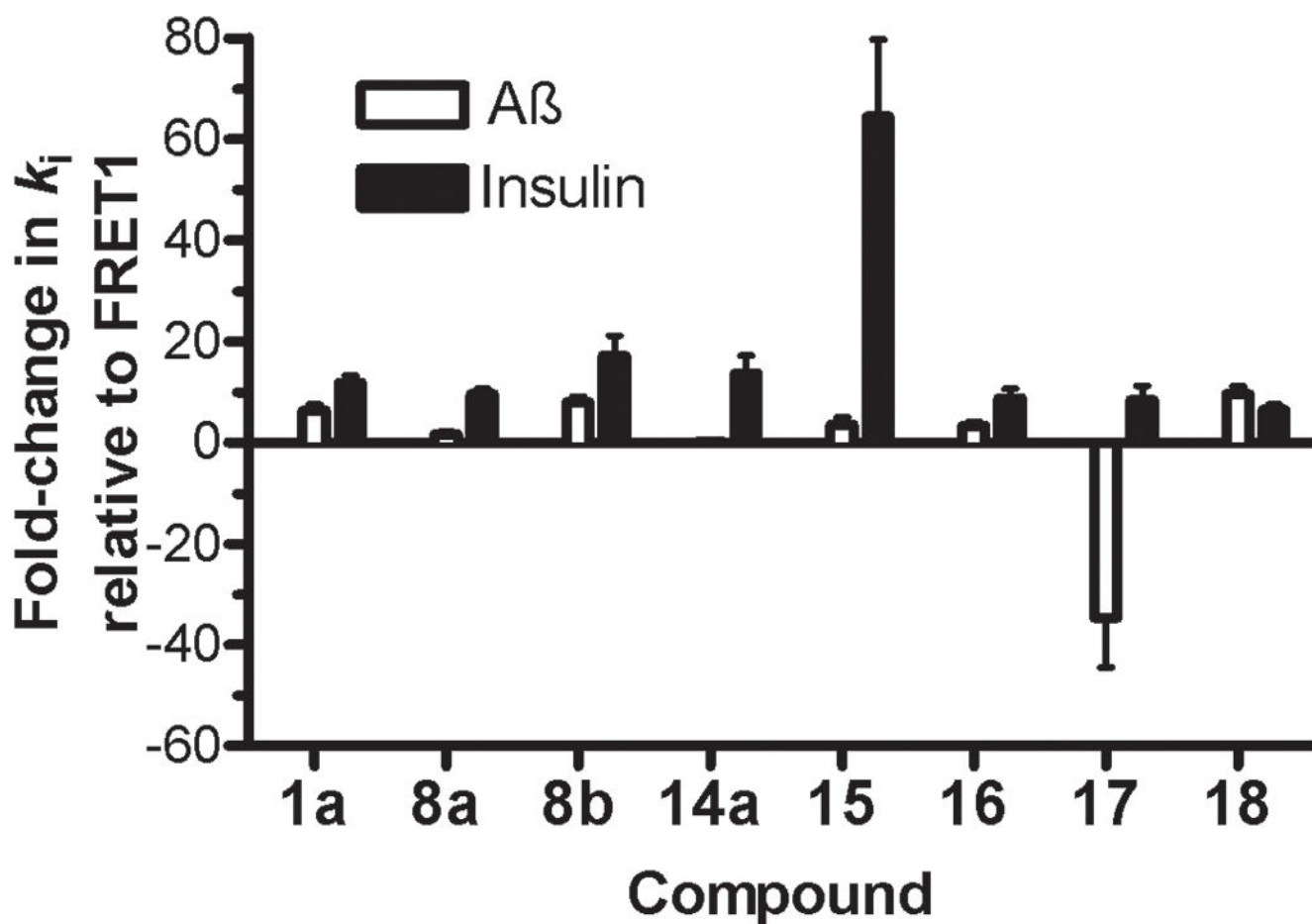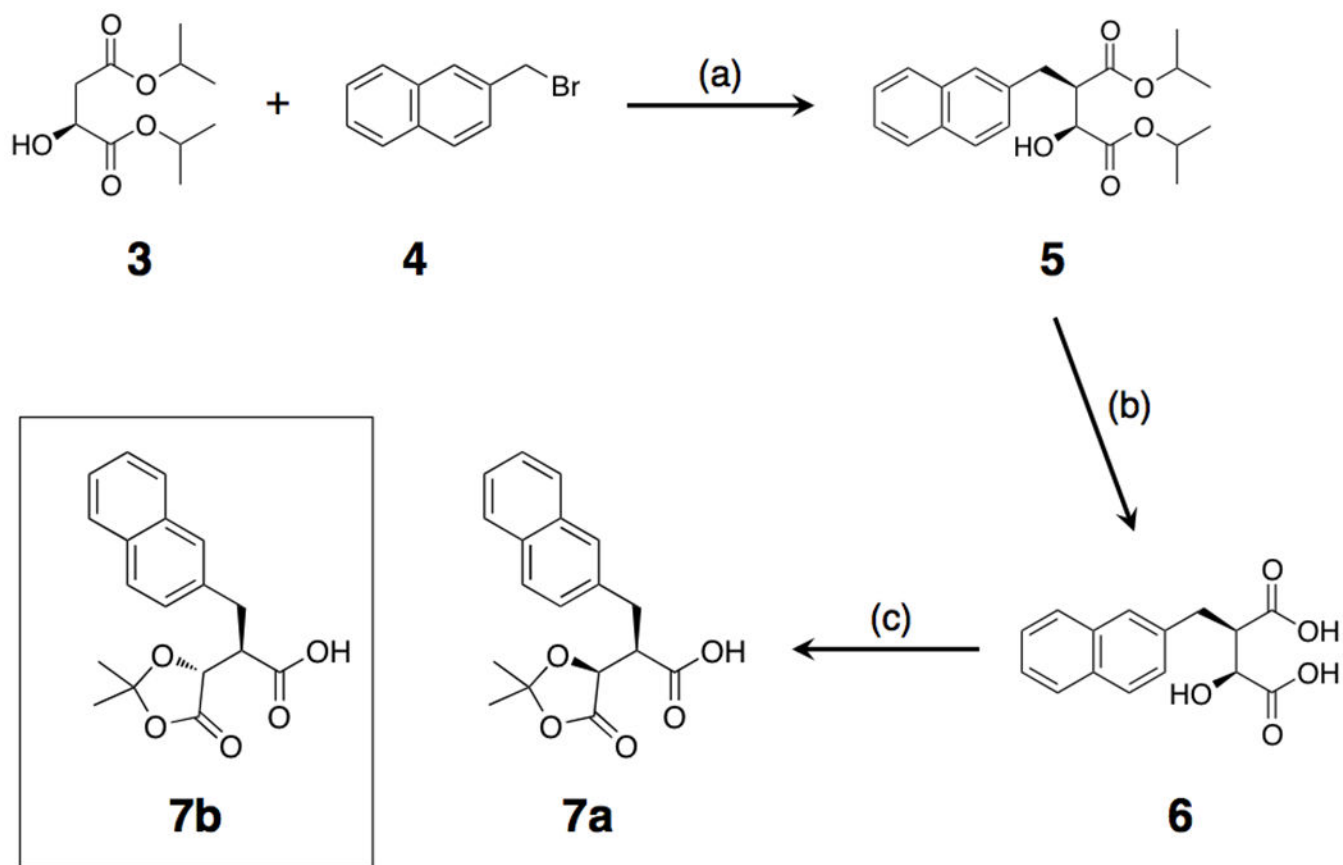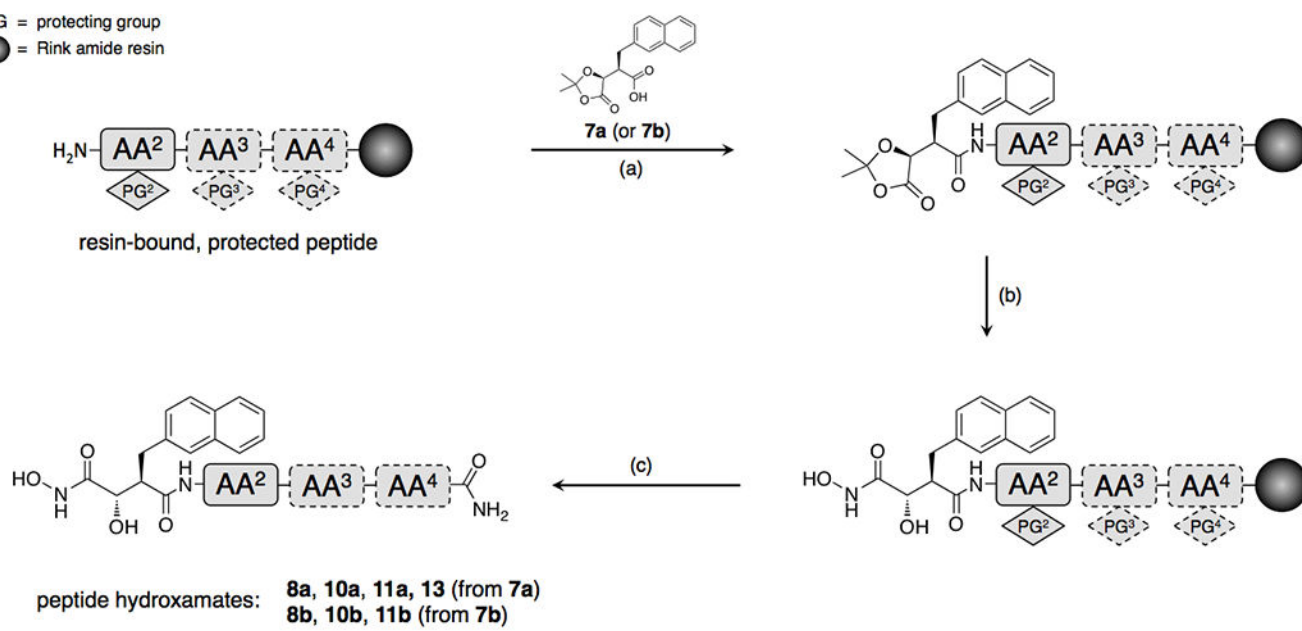
Figure 4.
The potency of individual IDE inhibitors is markedly substrate selective. Fold-change in apparent k_i (k_i^{app}) values for Aß degradation (*open bars*) and insulin degradation (*solid bars*) relative to those obtained with the FRET1 activity assay (derived from Table 5) obtained using inhibitor **1a** and the most potent inhibitors developed in this study. Note that most inhibitors show at least 10-fold higher k_i^{app} values for both Aß and insulin degradation relative to FRET1 degradation, an effect that nonetheless varies between different inhibitors. In particular, relative to FRET1 degradation, inhibitor **15** inhibits insulin degradation >60-fold, while inhibitor **17** inhibits the Aß degradation >30-fold more effectively.
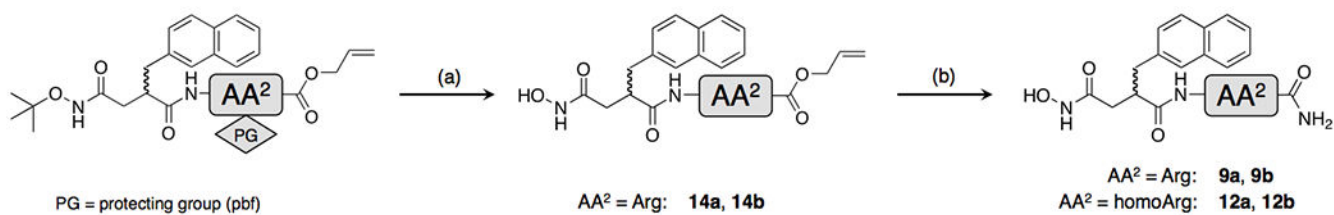
Scheme 1.

Scheme 2.

PG = protecting group (pbf)

AA² = Arg: **14a, 14b**

AA² = Arg: **9a, 9b**
AA² = homoArg: **12a, 12b**

Scheme 3.

Table 1.

Relative potency of 4-residue conventional peptide hydroxamate IDE inhibitors generated by alternate synthetic routes.
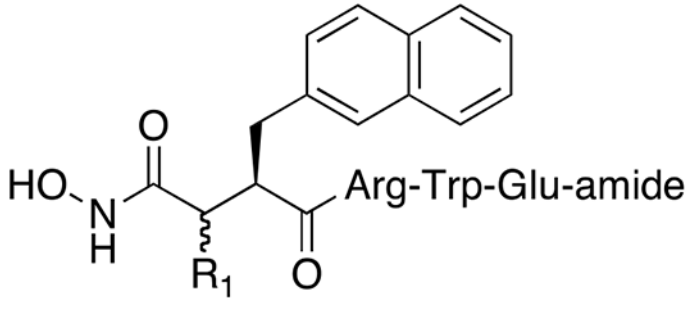

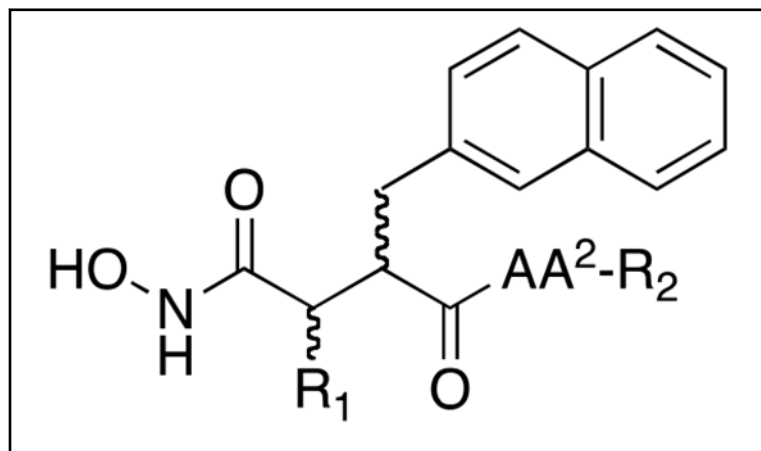| Cmpd.	R_1	R_1 (R/S)	k_i (nM) (FRET1)
1a	H	-	2.96 ± 0.20 (n = 3)
8a	OH	S	25.9 ± 1.2 (n = 3)
8b	OH	R	103 ± 6.9 (n = 3)

Table 2.

Effects of truncation on potency of conventional peptide hydroxamate IDE inhibitors.

Cmpd.	R_1	R_1 (R/S)	2Nap (R/S)	AA^2	AA^3	AA^4	k_i, nM (FRET1)
1a	H	-	R	Arg	Trp	Glu	2.96 ± 0.20 (n = 3)
9a	H	-	R	Arg	-	-	1150 ± 380 (n = 3)
1b	H	-	S	Arg	Trp	Glu	73.3 ± 40 (n = 3)
9b	H	-	S	Arg	-	-	>33000 (n = 3)
8a	OH	S	R	Arg	Trp	Glu	26.0 ± 1.2 (n = 3)
10a	OH	S	R	Arg	Trp	-	18000 ± 1100 (n = 3)
11a	OH	S	R	Arg	-	-	7750 ± 1600 (n = 3)
8b	OH	R	R	Arg	Trp	Glu	103 ± 7.0 (n = 3)
10b	OH	R	R	Arg	Trp	-	498 ± 10 (n = 3)
11b	OH	R	R	Arg	-	-	7020 ± 330 (n = 3)

Table 3.

Effects of modification of the P$_2$' moiety and terminal group on potency of conventional peptide hydroxamate IDE inhibitors.

Cmpd.	R$_1$	R$_1$ (R/S)	2Nap (R/S)	AA^2	R$_2$	k_i, nM (FRET1)
9a	H	-	R	Arg	NH$_2$	11,500 ± 380 (n = 3)
12a	H	-	R	homoArg	NH$_2$	>33,000 (n = 3)
9b	H	-	S	Arg	NH$_2$	>33,000 (n = 3)
12b	H	-	S	homoArg	NH$_2$	>33,000 (n = 3)
11a	OH	S	R	Arg	NH$_2$	7,750 ± 1600 (n = 3)
13	OH	S	R	homoArg	NH$_2$	>33,000 (n = 3)
14a	H	-	R	Arg	O-allyl	87 ± 11 (n = 3)
14b	H	-	S	Arg	O-allyl	5,280 ± 100 (n = 3)

Table 4.

Potency of retro-inverso peptide hydroxamates used for downstream characterization.

Cmpd.	Sequence	k_i, nM (FRET1)
15	*Glu-Trp-Arg-***2Nap**-Hx	49.8 ± 3.7 (n = 3)
16	*Glu-Tyr-Arg-***2Nap**-Hx	85.1 ± 5.0 (n = 3)
17	Ac-Glu(EDANS)-*Tyr-Bpa-***2Nap**-Hx	43.7 ± 8.0 (n = 3)
18	NH-*Asp-His-Phe-Ile-Arg-Glu-Trp-Arg-***2Nap**-Hx	23.1 ± 1.2 (n = 3)

2Nap = 2-naphthylalanine; Hx = hydroxamate; Ac = acetyl; EDANS = 5-((2-aminoethyl)amino)naphthalene-1-sulfonic acid; Bpa = benzoylphenylalanine. D-amino acids are shown in *italics*. ß-amino acids are shown in **bold text**. In compound **18**, the amino terminus is linked to the carboxylic acid residue in the Glu via a peptide bond.

Table 5.

The potency of active-site-directed IDE inhibitors varies in a substrate-selective manner.

Cmpd.	k_i^{app}, nM		
	FRET1	**FAßB**	**Insulin**
1a	2.96 ± 0.20 (n = 3)	21.7 ± 3.5 (n = 3)	37.9 ± 4.0 (n = 3)
8a	25.9 ± 1.2 (n = 3)	70.3 ± 12 (n = 3)	275 ± 25 (n = 3)
8b	103 ± 7.0 (n = 3)	927 ± 120 (n = 3)	1890 ± 410 (n = 3)
14a	86.9 ± 11 (n = 3)	107 ± 25 (n = 3)	1280 ± 300 (n = 3)
15	49.8 ± 3.7 (n = 3)	228 ± 67 (n = 3)	3260 ± 760 (n = 3)
16	85.1 ± 5.0 (n = 3)	365 ± 68 (n = 3)	833 ± 160 (n = 3)
17	43.7 ± 8.0 (n = 3)	1.40 ± 0.31 (n = 3)	410 ± 120 (n = 3)
18	23.1 ± 1.2 (n = 3)	246 ± 33 (n = 3)	171 ± 26 (n = 3)